



Effective Bipyridine and Pyrazine-Based Polysulfide Dissolution Resistant Complex Framework Material Systems for High Capacity Rechargeable Lithium–Sulfur Batteries

Pavithra M. Shanthi, Prashanth J. Hanumantha, Ramalinga Kuruba, Bharat Gattu, Moni K. Datta, and Prashant N. Kumta*

Lithium–sulfur (Li–S) batteries with high theoretical capacity ($\approx 1650 \text{ mAh g}^{-1}$) and specific energy density ($\approx 2567 \text{ Wh g}^{-1}$) have not achieved commercialization status due to low cycling stability arising from lithium polysulfide dissolution. Herein, sulfur infiltrated noncarbonized noncarbonate containing metal organic complex framework material (CFM) systems; sulfur-copper-bipyridine-CFM (S-Cu-bpy-CFM) and sulfur-copper-pyrazine-CFM (S-Cu-pyz-CFM) are developed as sulfur cathodes for the first time. The S-Cu-bpy-CFM and S-Cu-pyz-CFM show an initial capacity of 1626 and 1565 mAh g^{-1} with stable capacities of 1063 and 1025 mAh g^{-1} , respectively, after 150 cycles. An X-ray photoelectron spectroscopy (XPS) analysis after sulfur infiltration reveals the presence of —C—S— bonds arising from the Lewis acid–base interaction of the CFMs with sulfur. The battery separators cycled with the CMF cathodes display complete absence of polysulfides after 150 cycles. These CFM cathodes exhibit an initial fade in capacity during the first ≈ 25 cycles attributed to the irreversible reaction of nitrogen with sulfur (—N—S—) during cycling. A clear understanding of this chemical interaction between sulfur and nitrogen present in the sulfur-infiltrated CFMs is essential for engineering nitrogen containing hosts for trapping polysulfides effectively. Understanding reported here will lead to new materials for achieving the high specific energy densities characteristic to Li–S batteries.

batteries (LIBs). Commercial LIBs are ubiquitously known to store energy by reversibly intercalating lithium ions from a layered oxide cathode into a graphite anode exhibiting an energy density of 400 Wh kg^{-1} ,^[1] which is less than half of the current EV energy requirements.^[2] Research focused into developing new battery chemistries that can bypass the limitations of current LIBs has led to the identification and subsequent development of lithium–sulfur batteries (LSBs) as a promising technology. LSBs work based on a noninsertion-type crystallographic system presenting a two-electron redox reaction of one sulfur atom with two lithium ions, enabling the system to exhibit a high theoretical capacity and a specific energy of 1675 mAh g^{-1} ^[3] and 2600 Wh g^{-1} ,^[4] respectively. In addition, elemental sulfur offers additional advantages of low cost,^[5b] natural abundance,^[6] and environmental compatibility.^[7] Such benefits render the LSB to be a strong candidate for next-generation energy storage devices used for transportation and grid storage.

1. Introduction

Rapid progress in the development of next-generation electric vehicles (EVs) and hybrid EVs (HEVs) is largely limited by the saturated energy storage capacity of the existing lithium-ion

Despite the aforementioned advantages, LSBs face several challenges that need to be addressed, which include poor cyclability,^[8] low electrochemical utilization,^[9] inferior shelf life,^[10] and serious issues of self-discharge.^[11] These challenges arise primarily from the reaction of sulfur with lithium at the

P. M. Shanthi, B. Gattu, Prof. P. N. Kumta
Department of Chemical and Petroleum Engineering
University of Pittsburgh
815C Benedum Hall, 3700 O'Hara Street, Pittsburgh, PA 15261, USA
E-mail: pkumta@pitt.edu

Dr. P. J. Hanumantha, Dr. R. Kuruba, Dr. M. K. Datta, Prof. P. N. Kumta
Department of Bioengineering
University of Pittsburgh
Pittsburgh, PA 15261, USA

Prof. P. N. Kumta
Department of Mechanical Engineering and Materials Science
University of Pittsburgh
Pittsburgh, PA 15261, USA

Prof. P. N. Kumta
Center for Complex Engineered Multifunctional Materials
University of Pittsburgh
815C Benedum Hall, 3700 O'Hara Street, PA 15261, USA

The ORCID identification number(s) for the author(s) of this article can be found under <https://doi.org/10.1002/ente.201900141>.

DOI: 10.1002/ente.201900141

sulfur cathode and the successive changes in the physiochemical properties of the active materials and the electrolyte. Sulfur, as an electrode material, has poor electrical conductivity ($\approx 10^{-15} \text{ S m}^{-1}$),^[12] which greatly limits the utilization as an active material at the cathode, thus resulting in low electrochemical utilization.^[13] In addition, sulfur undergoes significant volume expansion (80%)^[14] during the electrochemical discharge-charge process that eventually leads to cracking and delamination of the cathode resulting in poor cyclability.^[15] Sulfur reacts with lithium ions to form a series of polysulfide intermediates (Li_2S_x , $x=1-8$) during the discharge cycle. These polysulfides, especially the species characterized by longer chain lengths, are highly soluble in the organic liquid electrolytes used in LSBs.^[16] This solubility of polysulfides is undesirable and results in uncontrolled leaching of active sulfur from the sulfur cathode, leading to crossover of the dissolved polysulfides toward the anode adding to the electrochemical impedance, ensuing polarization, and, finally, lowering the capacity and stability.^[17] The deposition of Li_2S and resulting polysulfides on the anode surface can impede the reversible charge transfer, thus limiting the overall capacity and power density.^[18] Polysulfide diffusion continues, even as the cell rests resulting in significant self-discharge contributing to poor shelf life that may not even last a single day.^[11]

To overcome these issues, a significant amount of research has been focused on the design and engineering of sulfur cathodes. The sulfur cathodes have shown a significant improvement in the electrochemical performance by the use of: 1) porous and functionalized conducting sulfur host,^[19] 2) additives to optimize the electrolyte properties,^[20] 3) modification of the current collector architecture,^[21] and 4) replacing the electrolyte-separator complex with a gel/composite/solid polymer electrolyte.^[22] By the implementation of these techniques, there have been reports of satisfactory improvements achieved in cell performance with stable capacities,^[23] albeit attaining the theoretical capacity of sulfur discussed earlier still remains elusive and largely impractical to achieve.

Of all the aforementioned strategies, the most effective and widely applied strategy is the impregnation of sulfur into a high surface area, electrical conductive carbon host.^[24] The use of conventional mesoporous^[25] and microporous^[26] carbonaceous materials with a high surface area^[27] and larger pore volume^[25a] has demonstrated the ability to hold large amounts of sulfur. However, the pores of these carbonaceous materials are subjected to clogging very easily after sulfur infiltration limiting the penetration of electrolyte, thus consequently reducing lithium-ion diffusion, and eventually leading to poor cycling performance.^[28] Carbon nanotube (CNT) and graphene form an open pore structure and have been found to be effective due to their high surface area^[29] and electrical conductivity.^[30] However, all these porous architectures exhibit a highly disordered^[31] and nontunable^[32] porous structure, which hinders complete prevention of polysulfide dissolution. Due to their highly tunable and ordered porous structure, metal organic frameworks (MOFs) have emerged as promising precursors for the preparation of porous carbon electrode hosts.^[33] MOFs are well designed assemblies of metal nodes coordinated to organic ligand linkers to form the 1D, 2D, or 3D structures. Hierarchical porous carbon templates derived from MOFs have

been used as sulfur hosts in LSBs with considerable improvement in the battery performance.^[26,33,34] Despite the highly tuned porous structure of these hosts derived from MOFs, they are inefficient in their ability to prevent the dissolution of polysulfide completely, primarily due to a lack of chemical interaction between the host and the resultant polysulfides.

Recently, the use of noncarbonized MOFs as sulfur immobilizing hosts in LSBs has attracted more interest.^[23a,35] Compared with traditional porous carbon structures, the metal nodes of the MOFs form Lewis acidic sites, and the functional groups from the organic moieties link to the Lewis basic sites serving as effective binding sites for the lithium polysulfides and strongly confining them within the MOFs, especially those nanosized porous framework complexes with rich cage-like structures, offering a platform for scientists to design materials for effectively restraining the dissolution and diffusion of polysulfides at the molecular level. Reports on using MOF as sulfur hosts have indeed taken advantage of the Lewis acid-base interaction of polysulfides with the binding functional sites.^[35,36] However, all these work on using noncarbonized MOFs reporting on the use of carboxylic acid ($-\text{CO}_2-$) functionalized organic linkers, and the corresponding electrochemical cycling plots show a significant drop in capacity during the first few cycles. For example, Wang et al.^[35b] used the Hong Kong University of Science and Technology (HKUST)-1 MOF derived from benzene-1,3,5-tricarboxylic acid linkers as sulfur hosts in LSBs. The MOFs showed an initial capacity of $\approx 1500 \text{ mAh g}^{-1}$, which quickly faded to $\approx 500 \text{ mAh g}^{-1}$ in the first 25 cycles. To explain this drop in capacity, we in our previous publication, Shanthi et al.^[37] used X-ray photoelectron spectroscopy (XPS) to analyze the chemical nature of the MOF-5 electrodes after electrochemical cycling and discovered the irreversible chemical interaction of carboxylate ($-\text{CO}_3-$) groups from the MOFs with sulfur to form sulfate, $-\text{SO}_4-$ moieties, rendering the MOFs electrochemically unstable. MOFs generated with the presence of $-\text{SO}_4-$ groups could be a possible solution to this issue. Accordingly, in this article, we have synthesized new complex framework materials (CFMs) utilizing sulfate-containing precursors.

The copper-sulfate-pyrazine CFM (Cu-pyz-CFM)^[38] and copper-sulfate-bipyridine CFM (Cu-bpy-CFM)^[39] are two such CFMs generated that contain the $-\text{SO}_4$ groups and were studied as sulfur hosts in this article for the first time. The CFMs were synthesized using simple hydrothermal techniques followed by sulfur infiltration under vacuum (**Figure 1**). The cathodes made from these sulfur infiltrated CFMs were tested for Li-S batteries. The S-CFMs upon testing exhibit an initial capacity of 1626 mAh g^{-1} (S-Cu-bpy-CFM) and 1565 mAh g^{-1} (S-Cu-pyz-CFM) and a stable capacity of $>1000 \text{ mAh g}^{-1}$ after 150 cycles. A loss in capacity is albeit observed during the initial stages of cycling, warranting further studies to be conducted that will help in understanding the underlying mechanisms involved in the cycling process. In this article, therefore, the cycling performance and the reasons contributing to the initial capacity loss along with the mechanisms responsible for the polysulfide dissolution were studied using XPS spectroscopy. The scientific findings from this article will help in not only designing but also developing new techniques to further enhance the cycling capacity as well as prevent the dissolution of polysulfides in Li-S battery cathodes.

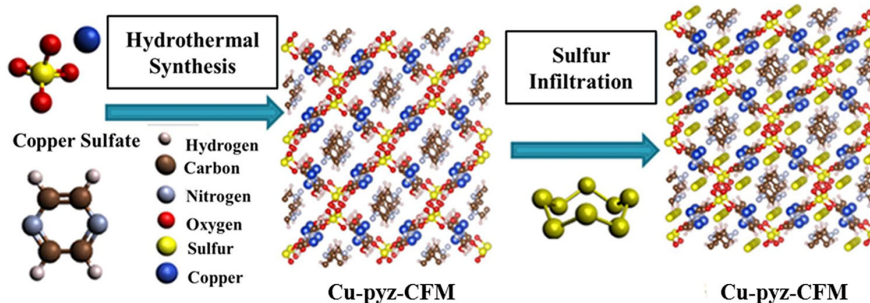


Figure 1. Scheme of the synthesis of Cu-pyz-CFM and sulfur infiltration.

2. Results and Discussion

The X-ray diffraction (XRD) analysis was performed on the as-synthesized Cu-pyz and Cu-bpy CFMs to confirm their phase purity. **Figure 2** shows the XRD patterns of the synthesized Cu-pyz-CFM and Cu-bpy-CFM compared with that simulated from their crystallographic information file (.cif) data. The crystallographic data files CCDC 636375^[38] and CCDC 805893^[39] corresponding to Cu-pyz-CFM and Cu-bpy-CFM, respectively, were extracted from the Cambridge Crystallographic Data Center (CCDC) (<https://www.ccdc.cam.ac.uk/structures/>) and used to simulate the XRD patterns of the CFMs using Materials Studio Materials Modelling and Simulation application by Accelrys Inc. The XRD pattern of the experimentally synthesized Cu-bpy-CFM and Cu-pyz-CFM matches well with the simulated patterns, confirming the single crystalline and phase-pure nature of the synthesized CFMs.

The synthesized CFMs similar to metal organic framework systems, MOFs, due to their highly ordered structure and fine-tuned porous nature, exhibit a high surface area.^[40] The surface area of the CFMs is a critical factor in accessing the extent of Lewis acid–base interaction between the CFMs and the polysulfides as well as eventual prevention of polysulfide dissolution.^[35a,41] In addition, data derived from the surface area analysis such as pore size and pore volume are important factors that decide

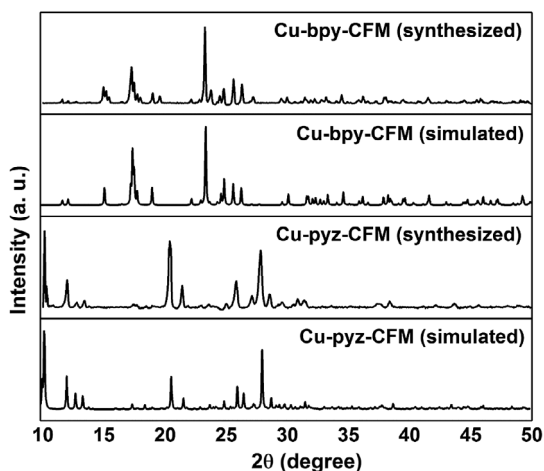


Figure 2. XRD patterns of experimentally synthesized Cu-pyz-CFM and Cu-bpy-CFM compared with the simulated XRD patterns.

the extent of successful infiltration of sulfur into the CFMs. The Brunauer–Emmett–Teller (BET) surface area analysis was performed on the CFMs to understand their nanoporous properties. **Table 1** represents the results of the pore size and surface area analysis, and Figure S1, Supporting Information, represents the adsorption isotherms corresponding to the Cu-bpy-CFM and Cu-pyz-CFM. The Cu-bpy-CFM and Cu-pyz-CFM exhibit a high BET surface area of ≈ 290.20 and $\approx 215.31 \text{ m}^2 \text{ g}^{-1}$, respectively. These values are typical of porous hosts used in the Li–S battery,^[23a,25a,26,28c] however, the CFMs synthesized herein have the additional advantage of exhibiting strong Lewis acid–base interaction characteristics. In addition, these CFMs have a very small pore size of $\approx 2.4\text{--}2.9 \text{ nm}$, which is in accordance with the values reported in the literature for nanoporous MOFs.^[42] This nanosized pore of the CFMs is expected to potentially aid in trapping and preventing the polysulfide species formed from dissolving into the electrolyte.

Sulfur was infiltrated into the CFMs using a vapor phase infiltration process.^[43] To confirm the nanoporous characteristic of the CFMs and the presence of crystalline sulfur inside the CFMs, transmission electron microscopy (TEM) analysis was conducted on the Cu-bpy-CFM and Cu-pyz-CFM samples following infiltration of sulfur. High- and low-resolution TEM micrographs of the CFMs are shown in **Figure 3**. The low-resolution TEM images of the CFMs (Figure 3a,c) clearly show the islands of sulfur generated inside the Cu-bpy-CFM and Cu-pyz-CFM crystals. The high-resolution images (Figure 3b,d), on the other hand, additionally clearly show the fringe patterns with a *d*-spacing of 0.204 nm corresponding to crystalline sulfur,^[43] confirming the infiltration of sulfur into the two CFM structures. In addition, the selected area electron diffraction (SAED) pattern of the sulfur infiltrated CFMs (inset of Figure 3b, d) also shows the diffraction pattern corresponding to crystalline

Table 1. Results of the BET surface and pore analysis of Cu-bpy-CFM and Cu-pyz-CFM. (Each datum is an average of three experiments conducted on three independent batches of synthesized Cu-bpy-CFM and Cu-pyz-CFM.)

Sample	BET surface area [$\text{m}^2 \text{ g}^{-1}$]	Langmuir surface area [$\text{m}^2 \text{ g}^{-1}$]	Total pore volume [$\text{cm}^3 \text{ g}^{-1}$]	Adsorption average pore width [nm]
Cu-bpy-CFM	290 ± 12	471 ± 22	0.31 ± 0.02	2.94 ± 0.22
Cu-pyz-CFM	215 ± 14	344 ± 34	0.32 ± 0.01	2.43 ± 0.18

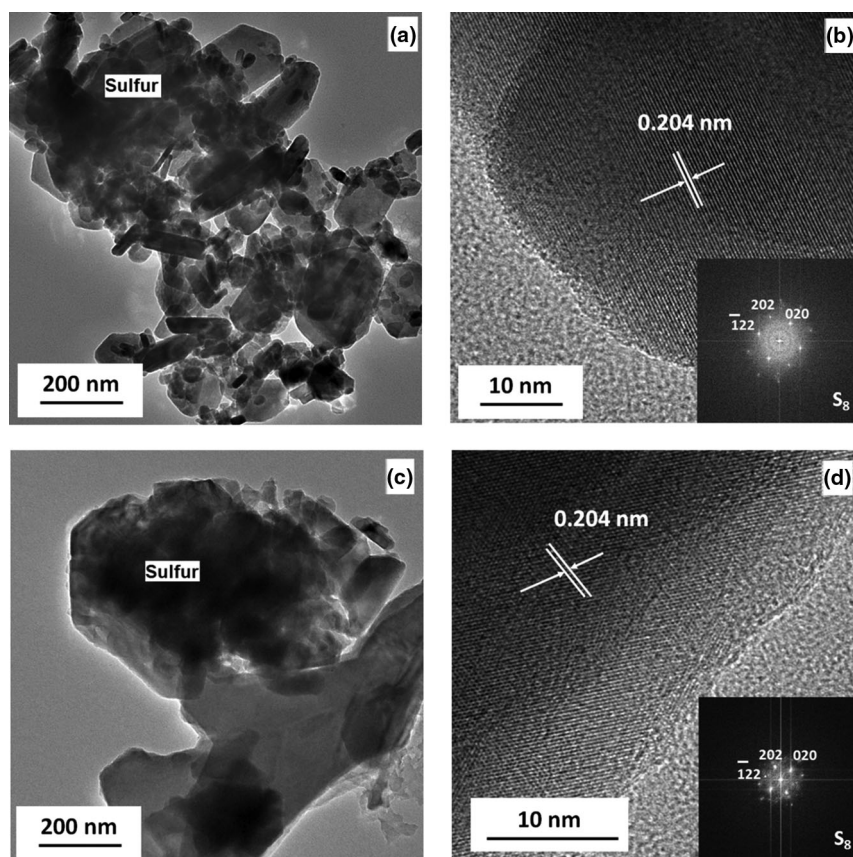


Figure 3. a,b) TEM images of S-Cu-bpy-CFM at two different magnifications along with the corresponding SAED pattern (Figure 3b, inset). c,d) TEM images of S-Cu-pyz-CFM at two different magnifications along with the corresponding SAED pattern (Figure 3d, inset).

sulfur planes of [122], [202], and [020].^[44] The synthesized CFMs were imaged using scanning electron microscopy (SEM), while the sulfur-infiltrated CFMs were also analyzed using the SEM and energy dispersive X-ray spectroscopy (EDS), and the results indicating the presence of sulfur validating the results of the TEM analyses presented earlier, are shown in Figure S2a–f and Table S1, Supporting Information.

The TEM and BET analyses presented earlier indicate that the infiltrated sulfur is likely present within the nanopores of the synthesized CFM. However, the presence of sulfur within and around the nanopores of the synthesized CFM cannot be discounted. The Lewis acid–base interactions generated indeed serve to preserve the electrochemical activity of the infiltrated sulfur as indicated by the electrochemical results discussed in the following sections.

The Fourier transform infrared spectroscopy (FTIR) analysis was performed on the CFMs after sulfur infiltration to understand the effect of the infiltration process and the nature of the chemical bonding in the CFMs before and after sulfur infiltration. A comparison of the FTIR spectra of Cu-bpy-CFM and Cu-pyz-CFM before and after sulfur infiltration is shown in **Figure 4**. The FTIR spectra of both the CFMs after sulfur infiltration retained all the peaks observed before sulfur infiltration, confirming the chemical stability of the CFMs after the sulfur-infiltration process.

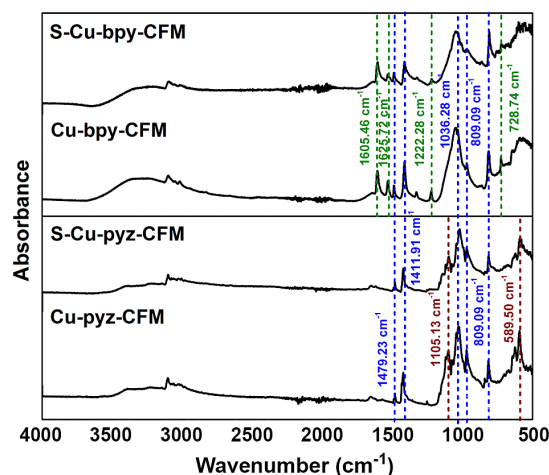


Figure 4. FTIR comparison of Cu-pyz-CFM and Cu-bpy-CFM before and after the sulfur infiltration process.

The CFMs show peaks at 1479.23 cm^{-1} (—C—C— stretching vibrations^[45]), 1411.91 cm^{-1} (—C—H— bending vibrations^[46]), 809.09 cm^{-1} (—C—C— stretching and coupled —C—H— deformation^[47]), 1036.28 cm^{-1} (—C—H— bending in ring

plane^[48]), and 809.209 cm^{-1} (—C—C— asymmetric stretching band^[49]). In addition to the common peaks, the Cu-bpy-CFM showed FTIR peaks at 1605.46, 1625.72, 1222.28, and 728.74 cm^{-1} corresponding to —C—O— stretching vibration,^[50] H—bonds involving —C—O— groups,^[51] symmetric stretching of —C—N— ,^[52] and out-of-plane —C—H— deformations,^[53] respectively. On the other hand, the Cu-pyz-CFM exhibited peaks at 1105.13 and 589.50 cm^{-1} arising from the —C—O— stretching^[54] and —C—N—C— vibrations,^[55] respectively. The absence of any anomalous peaks in the FTIR spectra validates the chemical stability of the CFMs after sulfur infiltration.

The TEM and SEM analyses of the S-Cu-bpy-CFM and S-Cu-pyz-CFM discussed earlier show the presence of crystalline sulfur inside the CFMs. The nature of sulfur binding was analyzed using the XPS spectroscopy. **Figure 5** shows the S2p spectra of commercial sulfur compared with that of S-Cu-bpy-CFM and S-Cu-pyz-CFM. Commercial sulfur exhibits S2p_{1/2} and S2p_{3/2} peaks at 164.70^[56] and 162.9 eV^[57] respectively.

However, the XPS spectra of the S-Cu-bpy-CFM and S-Cu-pyz-CFM show a shift in the S2p peaks, which upon careful comparison with the literature confirms the binding of sulfur to the carbon backbone of the CFM. Accordingly, the peaks at 164.40 and 163.20 eV correspond to —(C—S—O)— ^[58] binding and —(S—C)— ^[59] binding, respectively. The XPS analysis confirms the presence of a chemical binding between sulfur and carbon, which attribute to the likely binding and prevention of polysulfide dissolution. The absence of S2p at 164.7 eV in the XPS spectra collected on both, the Cu-bpy-CFM and Cu-pyz-CFM, confirms the absence of free sulfur S₈ in the synthesized CFMs and, hence, affirms the complete binding of the infiltrated sulfur to the carbon backbone in the synthesized CFM.

The effect of chemical binding between the CFMs and sulfur on the electrochemical performance of the S-CFMs was further studied by electrochemically cycling the S-Cu-bpy-CFM and S-Cu-pyz-CFM electrodes. **Figure 6a** shows the results of the electrochemical cycling experiments, and **Figure 6b** shows the rate capability experiments of S-Cu-bpy-CFM and S-Cu-pyz-CFM. (The cycling and rate capability experiments were performed on three batches of sulfur-infiltrated S-Cu-bpy-CFM and

S-Cu-pyz-CFM samples prepared independently from three batches of CFM samples. The difference in capacity observed in all the three runs was determined to be within $\pm 5\%$. Extended cycling of the S-Cu-bpy-CFM and S-Cu-pyz-CFM electrodes for 200 cycles is shown in **Figure S4**, Supporting Information.) The S-Cu-bpy-CFM shows an initial discharge capacity of 1565 mAh g^{-1} and stabilizes to a discharge capacity of 975 mAh g^{-1} after 200 cycles (fade rate of 0.19% per cycle). The S-Cu-pyz-CFM also shows a high initial discharge capacity of 1626 mAh g^{-1} and a stable discharge capacity of 1020 mAh g^{-1} after 200 cycles (fade rate of 0.18% per cycle). Both the S-Cu-bpy-CFM and S-Cu-pyz-CFM show good rate capability as seen from **Figure 6b**. This result is a significant improvement in performance as compared with the commercial sulfur cathodes that show an initial capacity of 697 mAh g^{-1} , which rapidly fades down to 57 mAh g^{-1} by the end of 150 charge–discharge cycles. **Table S2**, Supporting Information, shows a comparison of the performance of all the noncarbonized MOF-based cathode systems reported in the literature thus far. The current work on the S-Cu-bpy-CFM and S-Cu-pyz-CFM systems has the highest sulfur contents (49 wt%) in the cathode next to that reported by Zhao et al.^[60] in their work reported on MIL-101 (58.8 wt%) and Zheng et al.^[35a] on using Ni-MOF DUT-23 (60 wt%). The S-Cu-bpy-CFM and S-Cu-pyz-CFM systems used in the present work reported herein also show a very high stable discharge capacity of 975 and 1020 mAh g^{-1} , which is the highest value reported in the literature thus far to the best of our knowledge. The cycling stability of the S-Cu-bpy-CFM (0.19% per cycle) and S-Cu-pyz-CFM (0.18% per cycle) is also one of the lowest values reported in the literature so far. However, it is important to note that both the CFMs (S-Cu-bpy-CFM and S-Cu-pyz-CFM) exhibit a fade of $\approx 35\%$ of the initial discharge capacity during the initial ≈ 25 cycles followed by a stable cycling performance. To understand better and determine the exact reasons contributing to this fade in capacity, comprehensive XPS and FTIR analyses were performed on the electrodes and the separators before and after cycling. The results of the XPS analysis conducted on the separators clearly indicate the absence of polysulfides on the separators (**Figure 7**), thereby suggesting possible other reasons responsible for this observed initial loss in capacity. The separators following electrochemical cycling appeared identical in color to the pristine separators before cycling, visually also confirming the absence of polysulfides on the separators. The results of the XPS and FT-IR analyses conducted on the electrodes will be explained in detail in the following sections.

To further understand the electrochemical charge storage behavior of the S-CFMs and to identify the source of initial irreversible capacity loss, the charge–discharge profiles of the S-CFMs were evaluated and are shown in **Figure 6c** (S-Cu-bpy-CFM) and **Figure 6d** (S-Cu-pyz-CFM). **Figure 6c,d** corresponds to the specific capacity plots of 1st, 2nd, 10th, 25th, and 150th charge–discharge profiles of S-Cu-bpy-CFM and S-Cu-pyz-CFM at 0.2 C rate. The discharge profiles of both the CFMs show a smaller plateau at 2.35 V^[15] corresponding to the formation of the higher-order polysulfide during the initial stages of lithiation Li_2S_n ($n = 4–8$) and a wider plateau at 2.05 V^[61] that, in turn, corresponds to the formation of lower-order lithium sulfides Li_2S_n ($n < 4$). Similar plateaus at 2.4 and 2.25 V are observed in the charge cycles corresponding to the

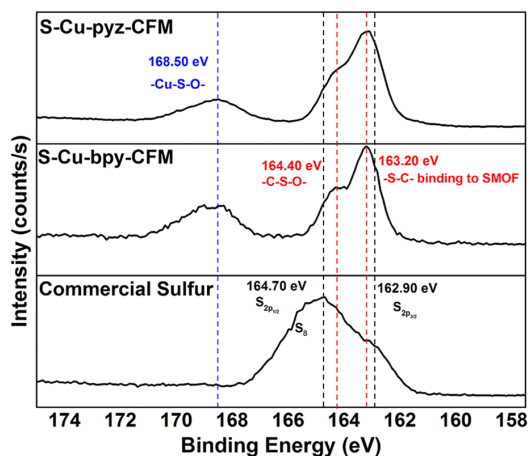


Figure 5. XPS S2p spectra of commercial sulfur, S-Cu-bpy-CFM, and S-Cu-pyz-CFM.

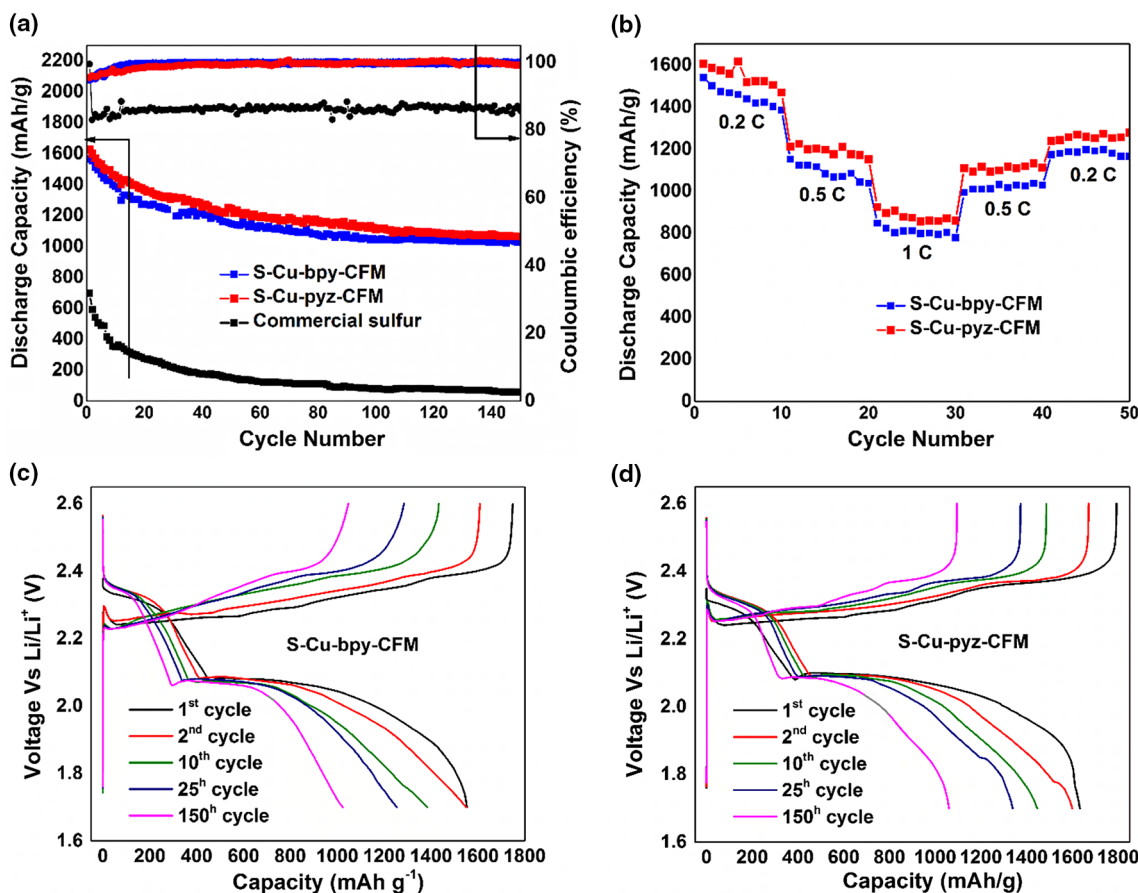


Figure 6. a) Cycling performance of S-Cu-bpy-CFM and S-Cu-pyz-CFM cycled at 0.2 C rate. b) Rate capability plot of S-Cu-bpy-CFM and S-Cu-pyz-CFM. c) Charge–discharge plot of S-Cu-bpy-CFM. d) Charge–discharge plot of S-Cu-pyz-CFM.

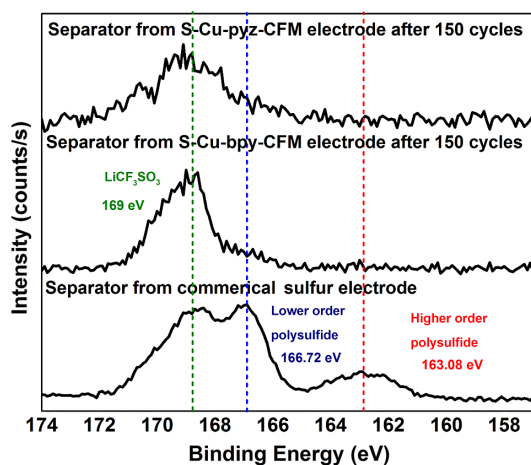


Figure 7. XPS S2p binding energy profile of separators from commercial sulfur electrode; S-Cu-bpy-CFM electrode and S-Cu-pyz-CFM electrode (after 150 cycles at 0.2 C rate).

delithiation of Li₂S to form the lower-order polysulfides and corresponding higher-order polysulfides, respectively, ultimately resulting in the formation of sulfur.

The cycling stability of the CFMs could be attributed to the nanoporous nature of their pores (Table 1) and chemical binding of sulfur to the carbon moieties of the CFMs as is evident from the XPS analysis (Figure 5). Though the S-CFMs exhibit an excellent initial discharge capacity and a good cycling stability, an initial loss of capacity is observed in the first 25 cycles. A similar kind of loss in capacity has been observed in the literature and is usually attributed to polysulfide dissolution into the electrolyte.^[62] However, the stable cycling performance observed after ≈25 cycles indicates the possibility of sulfur confinement by binding to the CFMs. This result implies that the origin of initial capacity loss needs to be studied in detail using the XPS and FTIR spectroscopy to understand the effectiveness of the Cu-bpy-CFM and Cu-pyz-CFM systems serving as effective polysulfide trapping agents in Li–S batteries.

To confirm the polysulfide trapping ability of the CFMs via Lewis acid–base interactions, the separators from the S-CFMs were analyzed using the XPS spectroscopy after 150 charge–discharge cycles. Figure 7 shows the S2p spectra of separators obtained from the cells cycled against commercial sulfur electrode compared with separators from the S-Cu-bpy-CFM and S-Cu-pyz-CFM electrodes after cycling for 150 cycles at 0.2 C rate.

The XPS spectra of the separator cycled against cathodes made from commercial sulfur (Figure 7) show S2p peaks at 168.90 eV,

which corresponds to the CF_3SO_3^- group from the electrolyte, along with peaks at 166.72 and 163.08 eV, clearly corresponding to the presence of lower- and higher-order polysulfides, respectively.^[63] This result confirms the ubiquitous and characteristic typical phenomenon of polysulfide dissolution observed in commercial sulfur cathodes during electrochemical charge-discharge cycles.

On the other hand, the separators corresponding to S-Cu-bpy-CFM and S-Cu-pyz-CFM after 150 cycles show only one S2p peak at 168.90 eV corresponding to the sulfur binding in LiCF_3SO_3 salt used in the electrolyte.^[59a] The absence of peaks corresponding to the polysulfides in the S-CFM separators post cycling indicates the complete entrainment of the polysulfide species by the CFMs. This can be attributed to the binding of the polysulfides due to the Lewis acid–base interactions between the synthesized CFMs and sulfur, as well as the entrapment effect provided by the nanoporous nature of the CFMs as is evident from the BET analysis (Table 1). There are also reports on the use of the carbonaceous porous matrix^[25,27a,64] including conventional carbonate-based MOFs^[35] as sulfur hosts that have shown improvement in electrochemical cycling. However, it should be noted that complete prevention of polysulfide dissolution has not been reported thus far, except for our previous work on the use of Zn-MOF-5^[37] as sulfur hosts in the Li–S battery. In our previous work, we unequivocally demonstrated total prevention of polysulfide dissolution, which was further confirmed by the XPS spectroscopy using a sulfur-infiltrated carbonate-based MOF, namely, Zn-MOF-5. However, despite being successful in trapping the polysulfide species, the Zn-MOF-5 was unstable under electrochemical charge–discharge conditions exhibiting a large capacity fade, particularly during the first ≈ 10 cycles attributed to the consumption of sulfur leading to the formation of sulfate species as indicated earlier.

The total absence of polysulfides confirmed by the XPS analysis conducted on the separators corresponding to S-Cu-bpy-CFM and Cu-pyz-CFM indeed makes them promising hosts for sulfur. However, the initial capacity loss observed during the charge–discharge cycling in these CFMs needs to be understood to effectively engineer these porous materials for further use as electrodes in the Li–S battery. The results of these studies are described in the following sections.

To explain the electrochemical cycling behavior of the CFMs, the electrodes from the Cu-bpy-CFM and Cu-pyz-CFM were further characterized using the XPS spectroscopy, both before and after 150 charge–discharge cycles. C1s spectra of the CFM electrodes before and after 150 charge–discharge cycles at 0.2 C rate are shown in **Figure 8**. Both the CFM electrodes exhibit the peak at 290.40 eV that represents the $-(\text{CF}_2-\text{CF}_2)-$ group arising from the polyvinylidene fluoride (PVdF) binder (289.87 eV),^[65] the peak at 286.10 eV corresponding to the $-(\text{C}-\text{S})-$ bond^[66] arising from the binding of sulfur to the ring carbon atoms, and the peak at 284.2 eV^[67] corresponding to other ring $-(\text{C}_6\text{H}_4\text{S})-$ bonds. The presence of these C–S peaks confirms the existence of sulfur–carbon binding observed in the S2p spectrum (Figure 5) and supports the findings that this chemical linkage between the sulfur and carbon species created during the sulfur infiltration process aids in polysulfide retention within the CFM structures. However, the CFM electrodes after 150 charge–discharge

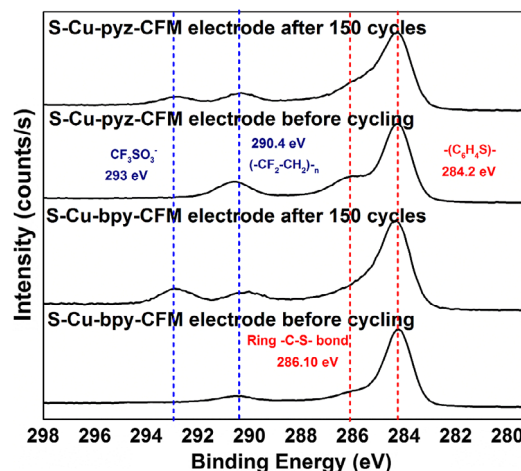


Figure 8. XPS C1s spectra of the S-Cu-bpy-CFM and S-Cu-pyz-CFM electrodes before and after 150 cycles at a rate of 0.2 C.

cycles at 0.2 C rate also show a peak at 293 eV in addition to the aforementioned peaks. This peak corresponds to the presence of the $-\text{CF}_3\text{SO}_3^-$ ^[59a] group originating from the lithium salt LiCF_3SO_3 used in the organic electrolyte. These results from the XPS analysis on the electrodes clearly show that there is no observable change in the binding of carbon atoms in the electrode, hence validating the stability of the carbon atoms in the synthesized CFM structures.

Cyclic voltammetry measurements were made on the S-Cu-bpy-CFM and S-Cu-pyz-CFM electrodes to provide a reasoning for the initial capacity loss. **Figure 9a,b** shows the cyclic voltammetry (CV) of the S-Cu-bpy-CFM and S-Cu-pyz-CFM electrodes performed at 0.05 mV s^{-1} scan rate. A change in the height of the peaks was observed in the CVs of both the S-Cu-bpy-CFM and S-Cu-pyz-CFM electrodes during the initial 25 charge–discharge cycles. This change in height could be related to polarization in the electrodes due to the possible insulating nature of the CFM structures and the observed loss in capacity during the first 25 cycles (see Table S3, Supporting Information, for a tabulated list of the peaks observed in both electrodes). However, the peaks corresponding to the 25th cycle and 30th cycle completely overlap each other, indicating that the loss in capacity is limited largely to the first 25 cycles only. The CV profiles show two cathodic peaks at 2.36 and 2.1 V corresponding to the lithiation of sulfur to form the higher and lower order polysulfides, respectively.^[68] The two anodic peaks at 2.38 and 2.43 eV correspond to the delithiation of the polysulfides^[69] to elemental sulfur and lithium through a series of higher and lower order polysulfides. The CV also shows an additional anodic peak at 2.19 eV, the intensity of which decreases and eventually disappears after the 25th cycle. This peak is, however, not observed in the cathodic scan, indicating the irreversible nature of the reaction corresponding to this peak. This reaction, if identified, could explain the initial irreversible capacity loss during the first 25 cycles.

The third peak at $\approx 2.19 \text{ V}$ in the CVs is believed to be arising from the irreversible binding of sulfur to the nitrogen moieties present in the CFMs. N1s scans of the XPS analysis were also

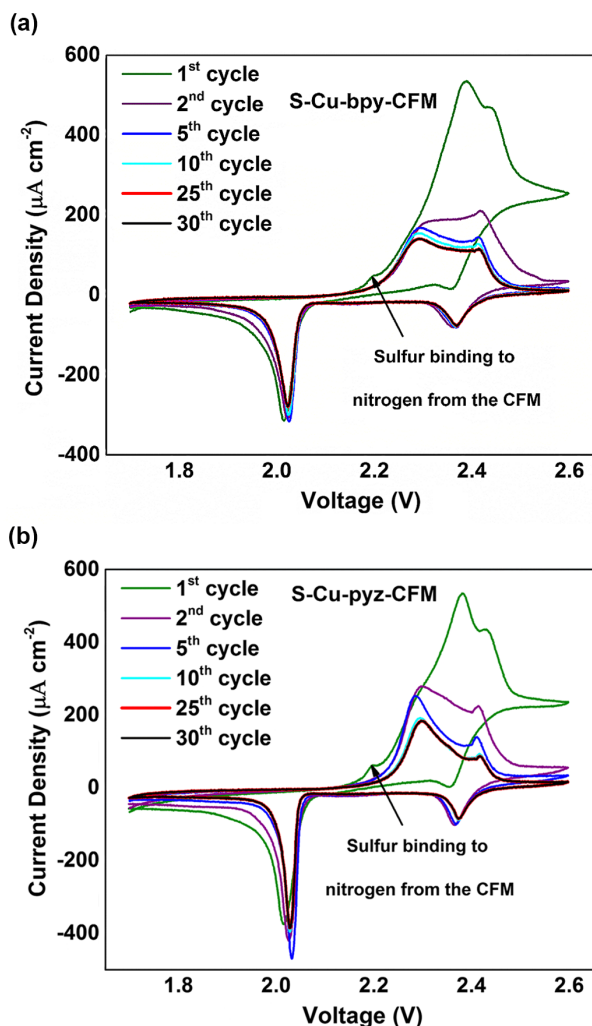


Figure 9. Cyclic voltammograms (CV) of a) S-Cu-bpy-CFM and b) S-Cu-pyz-CFM at different cycles performed at 0.05 mV s^{-1} scan rate.

collected and analyzed to ascertain if there is any evidence of —N—S— bonds. **Figure 10** shows the N1s spectra collected on the S-Cu-bpy-CFM and S-Cu-pyz-CFM electrodes before and after 150 charge–discharge cycles. The N1s spectra corresponding to the S-Cu-bpy-CFM and S-Cu-pyz-CFM after the 1st, 2nd, 10th, and 25th cycles are shown in Figure S4a,b, Supporting Information.

The N1s spectra of both S-Cu-bpy-CFM and S-Cu-pyz-CFM show a peak at 399.31 eV that corresponds to the binding of carbon to nitrogen arising from the —C—N—^[70] bonds of pyrazine and bipyridine present in the synthesized CFMs. A peak at 407.37 eV corresponding to LiNO_3 ^[71] added to the electrolyte is also observed in the electrodes cycled for 150 cycles and the corresponding electrodes after the 1st, 2nd, 10th, and 25th cycles (Figure S4a,b, Supporting Information). In addition to these peaks, the cycled electrodes show a peak at 403.52 eV, an analysis of which indicates its origin to the —N—S— bonds.^[72] Lalitha and Manoharan also observed similar peaks between nitrogen and sulfur while studying dithiolate complexes.^[73] Occurrence

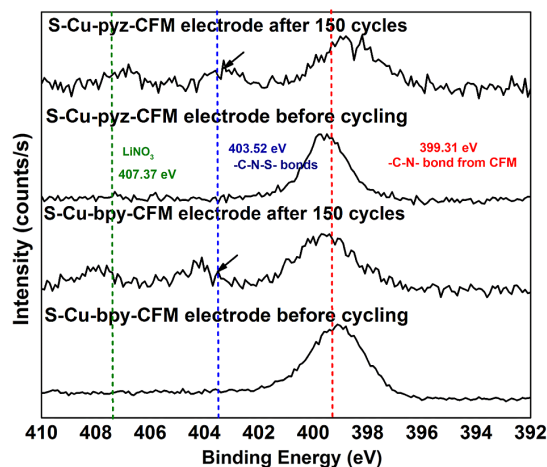


Figure 10. N1s spectra of S-Cu-bpy-CFM and S-Cu-pyz-CFM before and after 150 cycles (cycled at 0.2 C rate).

of this peak corresponding to the presence of —N—S— binding confirms our hypothesis and explains the initial loss in capacity to be attributed to the irreversible loss of sulfur caused by binding of the sulfur to nitrogen atoms from the CFM framework structure. Figure S4c, Supporting Information, also shows the presence of the peak at 403.52 eV in both the Cu-bpy-CFM and Cu-pyz-CFM electrodes after first charge and discharge confirming the irreversible nature of the —N—S— bond and justifies the corresponding loss in capacity.

From the results of the XPS analysis, the initial loss in capacity could arise from the irreversible chemical reaction between the sulfur and nitrogen atoms present in the two synthesized CFM structures (originating from the pyrazine and bipyridine subunits of the synthesized CFMs) rather than polysulfide dissolution. The amount of sulfur that is trapped by this irreversible —S—N— bond formed with the nitrogen in the CFMs on the basis of the initial stoichiometry used for sulfur infiltration into the CFMs indicates that ≈ 10 –15 wt% of the sulfur becomes inactive through binding with nitrogen present in the CFMs (Reactions S1 and S2, and Table S5, Supporting Information). This binding results in a ≈ 10 –15% loss in capacity during the initial 25 charge–discharge cycles. Furthermore, the XPS and FT-IR characterizations were performed on the S-Cu-bpy-CFM and S-Cu-pyz-CFM electrodes before and after cycling. The results account for the additional $\approx 20\%$ ($\approx 35\%$ total loss in capacity— $\approx 15\%$ due to N–S binding in the case of the S-Cu-pyz-CFM) and $\approx 25\%$ ($\approx 35\%$ total loss in capacity— $\approx 10\%$ due to N–S binding in the case of the S-Cu-bpy-CFM) loss in capacity.

XPS experiments were accordingly performed on the S-Cu-bpy-CFM and S-Cu-pyz-CFM electrodes before cycling and after the 1st, 2nd, 10th, 25th, and 150th cycles. **Figure 11a** represents the XPS S2p spectra collected on the S-Cu-bpy-CFM and S-Cu-pyz-CFM electrodes before and after 150 charge–discharge cycles. The S2p spectra of the S-Cu-bpy-CFM and S-Cu-pyz-CFM electrodes after the 1st, 2nd, 10th, and 25th cycles are shown in Figure S5a,b, Supporting Information. The S2p spectra collected on the S-Cu-bpy-CFM and S-Cu-pyz-CFM electrodes before cycling show peaks at 168.6 eV corresponding to the

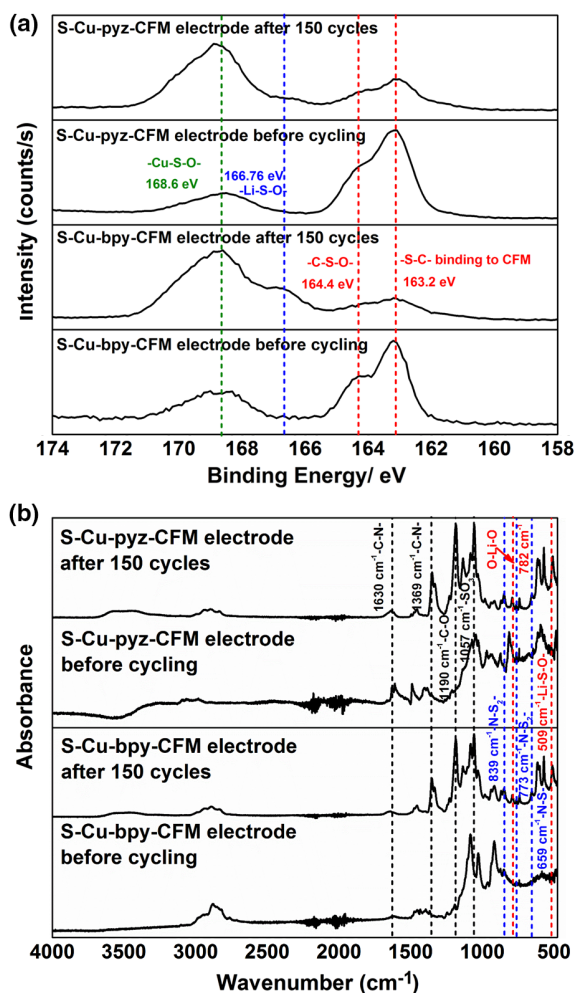


Figure 11. a) S2p spectra of S-Cu-bpy-CFM and S-Cu-pyz-CFM before and after 150 cycles (0.2 C rate). b) FT-IR spectra of the S-Cu-bpy-CFM and S-Cu-pyz-CFM before and after 150 cycles (0.2 C rate).

—Cu—S—O—^[74] linkages, which is a characteristic of the synthesized CFMs. The peaks observed at 163.2 and 164.4 eV in the spectra of S-Cu-bpy-CFM and S-Cu-pyz-CFM correspond to —C—S— bonds^[75] and —C—S—O—^[59a,76] bonds, respectively, formed due to the chemical interaction of sulfur with the carbon in the S-CFM. The S2p spectra collected on both the CFMs after 150 cycles (Figure 11a) (and after the 1st, 2nd, 10th, and 25th cycles as shown in Figure S5a,b, Supporting Information) show all the peaks observed before cycling, along with one additional peak at 166.76 eV corresponding to —Li—S—O—.^[77] This peak at 166.76 eV is likely due to the loss of active sulfur from the electrode due to formation of the well-known solid electrolyte interphase (SEI) layer, which could explain the additional $\approx 20\%$ loss in capacity in addition to the $\approx 15\%$ loss due to the formation of the —N—S— bonds. This SEI formed during the initial cycle is expected to stabilize the electrode, hence explaining the absence of a significant change in peak height in the CVs of the S-Cu-bpy-CFM and S-Cu-pyz-CFM (Figure 9a,b) after the 25th cycle. The presence of this peak at

166.76 eV in both the Cu-bpy-CFM electrode and Cu-pyz-CFM electrodes after the first charge and discharge (Figure S5c, Supporting Information) cycles confirms the irreversible nature of the SEI formed.

To further confirm the formation of the stable SEI layer in the form of —Li—S—O— compounds, the FT-IR analysis was also performed on the S-Cu-bpy-CFM and S-Cu-pyz-CFM electrodes before and after the 1st, 2nd, 10th, 25th, and 150th cycles. Figure 11b represents the FT-IR spectra collected on the S-Cu-bpy-CFM and S-Cu-pyz-CFM electrodes before and after 150 cycles. The FT-IR spectra collected on the S-Cu-bpy-CFM and S-Cu-pyz-CFM electrodes after the 1st, 2nd, 10th, and 25th cycles are shown in Figure S6a,b, Supporting Information. The FT-IR spectra collected on the S-Cu-bpy-CFM and S-Cu-pyz-CFM electrodes show the peak characteristics of the CFMs at 1027, 1079, 1395, and 1470 cm^{-1} corresponding to C—H rocking,^[78] C—C stretching,^[79] C—N^[80] bond stretching, and C—H bending vibrations,^[81] respectively. FT-IR peaks from Figure 11a are indexed in Table S4, Supporting Information. The S-Cu-bpy-CFM and S-Cu-pyz-CFM electrodes after cycling show peaks at 574 and 1057 cm^{-1} corresponding to CF₂ bending vibrations^[82–84] from the PVDF binder and —SO₃ groups from the LiCF₃SO₃ salt, respectively.^[85] These are in addition to the peak characteristics of the CFMs. In addition, the electrodes after cycling show peaks at 659, 773, and 839 cm^{-1} corresponding to the N—S symmetric stretching,^[86] N—S₂ asymmetric stretching,^[86] and N—S₂ stretching vibrations,^[87] respectively. These peaks arise from the binding of sulfur to nitrogen as demonstrated from the XPS N1s spectra from Figure 10. Two additional peaks are observed at 782 and 509 cm^{-1} that correspond to O—Li—O stretching^[88] and Li—S—O vibrations arising from cationic interaction with —SO₄ groups,^[89] respectively. The occurrence of these peaks corresponding to Li—S—O bonds in the FTIR spectra and XPS S2p spectra (Figure 11a and Figure S6a,b, Supporting Information) confirms the formation of SEI and subsequent loss of sulfur and $\approx 20\%$ loss in capacity. Figure S6c, Supporting Information, shows the FTIR spectra collected on the S-Cu-bpy-CFM and S-Cu-pyz-CFM after the first charge and the first discharge. The presence of peaks corresponding to —N—S— bond and Li—S—O bond in the FTIR spectra after the first charge and the first discharge indicates the irreversible nature of N—S bond and the SEI formed during cycling.

The results presented in this article, therefore, demonstrate the benefits of infiltrating sulfur into the nanoporous, metal sulfate-derived pyrazine and bipyridine CFM structures to ensure minimal polysulfide dissolution into the electrolyte ensuring minimal loss in capacity. This is due to the binding of carbon atoms from the CFM backbone with sulfur atoms, resulting in the prevention of the formed lithium polysulfide species from leaving the porous CFM matrix. However, it is also distinctly evident that the presence of nitrogen atoms in these two CFM structures contributes to the formation of —N—S— bonds during the initial charge–discharge cycles and SEI formation (Li—S—O), resulting in the loss of capacity during the initial stages of cycling and not due to the dissolved polysulfide species. The use of nitrogen-free sulfate/sulfonic CFMs as cathodes in the Li—S battery could help in improving the capacity along with cycling stability. Confirmation of the interaction between the sulfur and the nitrogen from the CFM structures aids in obtaining a better understanding of

the mechanisms involved in the lithiation of sulfur infiltrated into the chemically synthesized metal organic framework structures. The results presented in this article thus can further support the design of more efficient polysulfide-entrapping framework structures for achieving high energy density batteries in the Li–S system.

3. Conclusions

Metal sulfate containing nanoporous CFMs (Cu-bpy-CFM and Cu-pyz-CFM) were synthesized using microwave-assisted hydrothermal synthesis, followed by infiltration with sulfur, and used as cathodes to study their performance in the Li–S battery. The S-Cu-bpy-CFM shows an initial discharge capacity of 1565 mAh g⁻¹ and stabilizes at a discharge capacity of 975 mAh g⁻¹ after 200 cycles (fade rate of 0.19% per cycle). The S-Cu-pyz-CFM also shows a high initial discharge capacity of 1626 mAh g⁻¹ and a stable discharge capacity of 1020 mAh g⁻¹ after 200 cycles (fade rate of 0.18% per cycle). These CFMs interact with polysulfides via Lewis acid–base interactions, thereby effectively restraining the polysulfides from diffusing and dissolving into the electrolyte. In addition, the carbon atoms of the CFMs bind with sulfur during the sulfur infiltration process, further aiding in preventing the polysulfides from dissolving into the electrolyte. The XPS analysis of the CFM separators further confirms the absence of polysulfide dissolution. However, the observed loss in initial capacity is due to the irreversible binding of nitrogen from the CFMs to sulfur and SEI formation at the cathode as validated and explained by the XPS and FTIR analyses. This article thus provides an understanding of the ability of carbon-nitrogen containing porous complex metal organic frameworks based CFMs that were chemically synthesized to prevent polysulfide dissolution. The chemical insight gained from this work could help in employing these CFM systems as effective polysulfide trapping agents in the development of stable high capacity Li–S batteries in the near future.

4. Experimental Section

Materials: Copper(II) sulfate pentahydrate (CuSO₄·5H₂O, ≥98.0%, Sigma Aldrich), pyrazine (pyz, C₄H₄N₂, ≥99%, Sigma Aldrich), 4,4'-bipyridine (4,4'-bpy, C₁₀H₈N₂, ≥98.0%, Alfa Aesar), L-aspartic acid (L-asp, C₄H₇NO₄, ≥98%, Sigma Aldrich), benzoic acid (C₆H₅COOH, ≥99.5%, Sigma Aldrich), and sulfur (S, ≥99.5%, Sigma Aldrich) were the reagents used in the chemical synthesis of the CFMs, and all were used without further purification.

Synthesis of Cu-bpy-CFM: The Cu-bpy-CFM (Cu₂(4,4'-bpy)₂(SO₄)₂) was synthesized following a previous report by Shi et al.^[39] CuSO₄·5H₂O of 4.6 mmol (1.153 g), 4,4'-bpy of 6.6 mmol (1.030 g), and L-asp of 5.9 mmol (0.0787 g) were mixed in 160 mL of DI (deionized) water. The mixture was transferred to a microwave-assisted hydrothermal reactor and heated at 120 °C for 24 h. After the reaction, greenish yellow crystals obtained were filtered and washed with DI (deionized) water repeatedly before air-drying under ambient conditions.

Synthesis of Cu-pyz-CFM: The Cu-pyz-CFM (Cu₂(pyz)₂(SO₄)₂) was synthesized per earlier report by Amo-Ochoa et al.^[38] A precursor mixture of 6.264 mmol (1.564 g) CuSO₄·5H₂O, 6.264 mmol (0.502 g) pyz, and 6.264 mmol (0.762 g) C₆H₅COOH were mixed in 30 mL of deionized water. The reaction mixture was heated at 180 °C for 12 h in a

microwave-assisted hydrothermal furnace to obtain red crystals of Cu-pyz-CFM. The resulting red crystals were filtered on a glass frit, washed with warm water, and dried under ambient air.

Sulfur Infiltration into the CFMs: The CFMs were dried under vacuum conditions at 100 °C for 12 h to remove residual solvent and the water of crystallization from the synthesis process. The synthesized CFMs were infiltrated with sulfur under vacuum, following the procedure reported by the authors earlier in their previous work on S-Zn-CFM.^[37] Sulfur and CFM weights (70:30 wt%) calculated considering the stoichiometry and pore volume data (see Supporting Information) were sealed under vacuum into a quartz tube and then heated at 300 °C for 24 h to prepare the sulfur infiltrated S-Cu-pyz-CFM and S-Cu-bpy-CFM.

Chemical and Electrochemical Characterization: The crystal structure of the Cu-bpy-CFM and Cu-pyz-CFM before and after sulfur infiltration was analyzed using the XRD spectroscopy in a Philips XPERT PRO system that uses Cu Kα (λ = 0.15406 nm) radiation. The samples were scanned in the range of 10°–90° (2θ) under a constant current and voltage of 40 mA and 45 kV, respectively. The SEM images of the CFMs were obtained using a Philips XL30 machine at 10 kV. An attenuated total reflectance Fourier transform IR spectroscope (ATR-FTIR, Nicolet 6700 Spectrophotometer, Thermo Electron Corporation), which uses a diamond ATR smart orbit, was used to obtain the FT-IR spectra of the samples. The FTIR spectra are collected at a resolution of 1 cm⁻¹, averaging 32 scans between the frequency of 400 and 4000 cm⁻¹. The XPS analyses of the CFMs and S-CFMs were performed using the ESCALAB 250 Xi system (Thermo Scientific). This XPS system consists of the monochromated Al Kα X-ray source and low-energy (<10 eV) argon ions and low-energy electron beams that provide the charge neutralization. The XPS measurements were carried out at room temperature, under an ultra-high vacuum (UHV) chamber (<5 × 10⁻¹⁰ mBar) employing a spot size of 200 × 200 μm². The surface area and pore characteristics of all the CFM samples were analyzed using a Micromeritics ASAP 2020 Physisorption analyzer, using the BET isotherm generated.

The S-CFMs were cycled between 1.7 and 2.6 V (with respect to Li⁺/Li) at a current rate of 0.2 C (≈330 mA g⁻¹) in a 2025-coin cell using the Arbin BT200 battery testing station to evaluate their electrochemical performance. The cathodes for electrochemical evaluation were prepared by manually coating a dispersion of 70 wt% S-CFMs, 20 wt% acetylene black, and 10 wt% PVDF dispersed in *N*-methyl pyrrolidone (NMP) on an aluminum foil, followed by vacuum drying for 12 h at 60 °C. All the cathodes that were tested had a uniform sulfur loading of 1.5–2 mg cm⁻². Accordingly, 2025-coin cells were assembled with the S-CFM coated cathodes as the working electrode, a lithium foil as the counter electrode, and Celgard 2400 polypropylene (PP) as the separator in an Innovative, Inc. glove box (UHP Argon, <0.1 ppm O₂, H₂O). A 1 M LiCF₃SO₃ (lithium trifluoromethanesulfonate) and 0.2 M LiNO₃ dissolved in 50:50 vol% 1,3 dioxolane and 1,2 dimethoxyethane were used as the electrolytes. The CV measurements were performed on the cells in a VersaSTAT3 electrochemical workstation, Princeton Applied Research in the voltage range of 1.7–2.6 V at a slow scan rate of 0.1 mV s⁻¹.

Supporting Information

Supporting Information is available from the Wiley Online Library or from the author.

Acknowledgements

This research was funded by the U.S. Department of Energy (DE-EE0006825, DE-EE0007797, and DE-EE0008199), the Edward R. Weidlein Chair Professorship Funds, and the Center for Complex Engineered Multifunctional Materials (CCEMM), Swanson School of Engineering at the University of Pittsburgh. The authors acknowledge Dr. Joel Gillespie from the PPG Materials Characterization Laboratory (Department of Chemistry, University of Pittsburgh) for providing access to the XPS instrumentation. Mr. Louis Wang (Department of Energy, Environmental and Chemical Engineering, Washington University in St. Louis) is also acknowledged for

his assistance in conducting experiments during the initial stages of this research. Additionally, Dr. John A. Keith and Mr. Karthikeyan Saravanan from the Department of Chemical Engineering, University of Pittsburgh are acknowledged for their help with simulating the XRD patterns collected of the CFMs from the CIF (Crystallographic Information File) information.

Conflicts of Interest

The authors declare no conflict of interest.

Keywords

lithium–sulfur batteries, noncarbonized sulfate CFM, polysulfide encapsulation

Received: February 1, 2019

Revised: March 11, 2019

Published online: May 16, 2019

- [1] a) Y. Yang, G. Zheng, Y. Cui, *Chem. Soc. Rev.* **2013**, *42*, 3018; b) M.-K. Song, Y. Zhang, E. J. Cairns, *Nano Lett.* **2013**, *13*, 5891.
- [2] a) M. Ehsani, Y. Gao, S. Longo, K. Ebrahimi, *Modern Electric, Hybrid Electric, and Fuel Cell Vehicles*, CRC Press, Boca Raton, FL **2018**; b) L. Zhang, X. Hu, Z. Wang, F. Sun, J. Deng, D. G. Dorrell, *IEEE Trans. Veh. Technol.* **2018**, *67*, 1027.
- [3] N. Nitta, F. Wu, J. T. Lee, G. Yushin, *Mater. Today* **2015**, *18*, 252.
- [4] A. Manthiram, S. H. Chung, C. Zu, *Adv. Mater.* **2015**, *27*, 1980.
- [5] a) J. Kim, D. J. Lee, H. G. Jung, Y. K. Sun, J. Hassoun, B. Scrosati, *Adv. Funct. Mater.* **2013**, *23*, 1076; b) A. Manthiram, S. H. Chung, C. Zu, *Adv. Mater.* **2015**, *27*, 1980.
- [6] V. S. Kolosnitsyn, E. V. Karaseva, *Russ. J. Electrochem.* **2008**, *44*, 506.
- [7] U. Hofer, *Nat. Rev. Microbiol.* **2018**, *16*, 260.
- [8] R. Fang, S. Zhao, Z. Sun, D. W. Wang, H. M. Cheng, F. Li, *Adv. Mater.* **2017**, *29*, 1606823.
- [9] Y. X. Yin, S. Xin, Y. G. Guo, L. J. Wan, *Angew. Chem., Int. Ed.* **2013**, *52*, 13186.
- [10] Y. V. Mikhaylik, J. R. Akridge, *J. Electrochem. Soc.* **2004**, *151*, A1969.
- [11] L. Wang, J. Liu, S. Yuan, Y. Wang, Y. Xia, *Energy Environ. Sci.* **2016**, *9*, 224.
- [12] M. Edeling, R. W. Schmutzler, F. Hensel, *Phil. Mag. Part B* **1979**, *39*, 547.
- [13] Z. W. Seh, Y. Sun, Q. Zhang, Y. Cui, *Chem. Soc. Rev.* **2016**, *45*, 5605.
- [14] D.-W. Wang, Q. Zeng, G. Zhou, L. Yin, F. Li, H.-M. Cheng, I. R. Gentle, G. Q. M. Lu, *J. Mater. Chem. A* **2013**, *1*, 9382.
- [15] N. Ding, L. Zhou, C. Zhou, D. Geng, J. Yang, S. W. Chien, Z. Liu, M. F. Ng, A. Yu, T. S. A. Hor, *Sci. Rep.* **2016**, *6*, 33154.
- [16] L. Ming, L. Qing, Q. Xianying, L. Gemeng, H. Wenjie, Z. Dong, H. Yan-Bing, L. Baohua, K. Feiyu, *Small* **2017**, *13*, 1602539.
- [17] T. Yim, M.-S. Park, J.-S. Yu, K. J. Kim, K. Y. Im, J.-H. Kim, G. Jeong, Y. N. Jo, S.-G. Woo, K. S. Kang, I. Lee, Y.-J. Kim, *Electrochim. Acta* **2013**, *107*, 454.
- [18] a) Y. Fu, Y. S. Su, A. Manthiram, *Angew. Chem., Int. Ed.* **2013**, *52*, 6930; b) J. Zheng, M. Gu, H. Chen, P. Meduri, M. H. Engelhard, J.-G. Zhang, J. Liu, J. Xiao, *J. Mater. Chem. A* **2013**, *1*, 8464.
- [19] a) C. B. Bucur, J. Muldoon, A. Lita, *Energy Environ. Sci.* **2016**, *9*, 992; b) G. Zhou, E. Paek, G. S. Hwang, A. Manthiram, *Nat. Commun.* **2015**, *6*, 7760; c) X. Liang, Y. Rangom, C. Y. Kwok, Q. Pang, L. F. Nazar, *Adv. Mater.* **2017**, *29*, 1603040.
- [20] a) S. Liu, G. R. Li, X. P. Gao, *ACS Appl. Mater. Interfaces* **2016**, *8*, 7783; b) X. B. Cheng, C. Yan, J. Q. Huang, P. Li, L. Zhu, L. Zhao, Y. Zhang, W. Zhu, S. T. Yang, Q. Zhang, *Energy Storage Mater.* **2017**, *6*, 18.
- [21] a) H. J. Peng, W. T. Xu, L. Zhu, D. W. Wang, J. Q. Huang, X. B. Cheng, Z. Yuan, F. Wei, Q. Zhang, *Adv. Funct. Mater.* **2016**, *26*, 6351; b) Q. Li, S. Zhu, Y. Lu, *Adv. Funct. Mater.* **2017**, *27*, 1606422.
- [22] a) M. Rao, X. Geng, X. Li, S. Hu, W. Li, *J. Power Sources* **2012**, *212*, 179; b) M. Liu, D. Zhou, Y.-B. He, Y. Fu, X. Qin, C. Miao, H. Du, B. Li, Q.-H. Yang, Z. Lin, T. S. Zhao, F. Kang, *Nano Energy* **2016**, *22*, 278; c) K. Murata, S. Izuchi, Y. Yoshihisa, *Electrochim. Acta* **2000**, *45*, 1501; d) Q. Guo, Y. Han, H. Wang, X. Hong, C. Zheng, S. Liu, K. Xie, *RSC Adv.* **2016**, *6*, 101638.
- [23] a) X.-J. Hong, T.-X. Tan, Y.-K. Guo, X.-Y. Tang, J.-Y. Wang, W. Qin, Y.-P. Cai, *Nanoscale* **2018**, *10*, 2774; b) X. Zhang, W. Wang, A. Wang, Y. Huang, K. Yuan, Z. Yu, J. Qiu, Y. Yang, *J. Mater. Chem. A* **2014**, *2*, 11660; c) J. Q. Huang, Q. Zhang, H. J. Peng, X. Y. Liu, W. Z. Qian, F. Wei, *Energy Environ. Sci.* **2014**, *7*, 347; d) G. Ma, Z. Wen, M. Wu, C. Shen, Q. Wang, J. Jin, X. Wu, *Chem. Commun.* **2014**, *50*, 14209; e) J. S. Kim, T. H. Hwang, B. G. Kim, J. Min, J. W. Choi, *Adv. Funct. Mater.* **2014**, *24*, 5359.
- [24] L. Borchardt, M. Oschatz, S. Kaskel, *Chem. – Eur. J.* **2016**, *22*, 7324.
- [25] a) B. Ding, C. Yuan, L. Shen, G. Xu, P. Nie, X. Zhang, *Chem. – Eur. J.* **2013**, *19*, 1013; b) D. Li, F. Han, S. Wang, F. Cheng, Q. Sun, W.-C. Li, *ACS Appl. Mater. Interfaces* **2013**, *5*, 2208; c) X. Liang, Z. Wen, Y. Liu, H. Zhang, L. Huang, J. Jin, *J. Power Sources* **2011**, *196*, 3655.
- [26] H. B. Wu, S. Wei, L. Zhang, R. Xu, H. H. Hng, X. W. Lou, *Chem. – Eur. J.* **2013**, *19*, 10804.
- [27] a) Z. Gong, Q. Wu, F. Wang, X. Li, X. Fan, H. Yang, Z. Luo, *RSC Adv.* **2016**, *6*, 37443; b) J. Schuster, G. He, B. Mandlmeier, T. Yim, K. T. Lee, T. Bein, L. F. Nazar, *Angew. Chem., Int. Ed.* **2012**, *51*, 3591.
- [28] a) Z. Juan, Y. Chun-Peng, Y. Ya-Xia, W. Li-Jun, G. Yu-Guo, *Adv. Mater.* **2016**, *28*, 9539; b) H. Sohn, M. L. Gordin, T. Xu, S. Chen, D. Lv, J. Song, A. Manivannan, D. Wang, *ACS Appl. Mater. Interfaces* **2014**, *6*, 7596; c) J. Zheng, G. Guo, H. Li, L. Wang, B. Wang, H. Yu, Y. Yan, D. Yang, A. Dong, *ACS Energy Lett.* **2017**, *2*, 1105.
- [29] H. J. Peng, J. Q. Huang, M. Q. Zhao, Q. Zhang, X. B. Cheng, X. Y. Liu, W. Z. Qian, F. Wei, *Adv. Funct. Mater.* **2014**, *24*, 2772.
- [30] H. Wang, Y. Yang, Y. Liang, J. T. Robinson, Y. Li, A. Jackson, Y. Cui, H. Dai, *Nano Lett.* **2011**, *11*, 2644.
- [31] X. Li, Y. Cao, W. Qi, L. V. Saraf, J. Xiao, Z. Nie, J. Mietek, J.-G. Zhang, B. Schwenzer, J. Liu, *J. Mater. Chem.* **2011**, *21*, 16603.
- [32] J. Wang, S. Y. Chew, Z. W. Zhao, S. Ashraf, D. Wexler, J. Chen, S. H. Ng, S. L. Chou, H. K. Liu, *Carbon* **2008**, *46*, 229.
- [33] K. Xi, S. Cao, X. Peng, C. Ducati, R. Vasant Kumar, A. K. Cheetham, *Chem. Commun.* **2013**, *49*, 2192.
- [34] G. Xu, B. Ding, L. Shen, P. Nie, J. Han, X. Zhang, *J. Mater. Chem. A* **2013**, *1*, 4490.
- [35] a) J. Zheng, J. Tian, D. Wu, M. Gu, W. Xu, C. Wang, F. Gao, M. H. Engelhard, J.-G. Zhang, J. Liu, J. Xiao, *Nano Lett.* **2014**, *14*, 2345; b) Z. Wang, X. Li, Y. Cui, Y. Yang, H. Pan, Z. Wang, C. Wu, B. Chen, G. Qian, *Cryst. Growth Des.* **2013**, *13*, 5116.
- [36] H. Park, D. J. Siegel, *Chem. Mater.* **2017**, *29*, 4932.
- [37] P. M. Shanthi, P. J. Hanumantha, B. Gattu, M. Sweeney, M. K. Datta, P. N. Kumta, *Electrochim. Acta* **2017**, *229*, 208.
- [38] P. Amo-Ochoa, G. Givaja, P. J. S. Miguel, O. Castillo, F. Zamora, *Inorg. Chem. Commun.* **2007**, *10*, 921.
- [39] F.-N. Shi, A. R. Silva, J. Rocha, *J. Solid State Chem.* **2011**, *184*, 2196.
- [40] a) O. K. Farha, I. Eryazici, N. C. Jeong, B. G. Hauser, C. E. Wilmer, A. A. Sarjeant, R. Q. Snurr, S. T. Nguyen, A. Ö. Yazaydin, J. T. Hupp, *J. Am. Chem. Soc.* **2012**, *134*, 15016; b) B. Li, H.-M. Wen, W. Zhou, Jeff Q. Xu, B. Chen, *Chem* **2016**, *1*, 557.
- [41] a) L. Liang, C. Liu, F. Jiang, Q. Chen, L. Zhang, H. Xue, H.-L. Jiang, J. Qian, D. Yuan, M. Hong, *Nat. Commun.* **2017**, *8*, 1233;

- b) C.-H. Lim, A. M. Holder, J. T. Hynes, C. B. Musgrave, *Inorg. Chem.* **2013**, *52*, 10062.
- [42] a) X. Zhao, B. Xiao, A. J. Fletcher, K. M. Thomas, D. Bradshaw, M. J. Rosseinsky, *Science* **2004**, *306*, 1012; b) X. Lin, I. Telepeni, A. J. Blake, A. Dailly, C. M. Brown, J. M. Simmons, M. Zoppi, G. S. Walker, K. M. Thomas, T. J. Mays, P. Hubberstey, N. R. Champness, M. Schröder, *J. Am. Chem. Soc.* **2009**, *131*, 2159; c) R. Q. Snurr, J. T. Hupp, S. T. Nguyen, *AIChE J.* **2004**, *50*, 1090; d) A. J. Fletcher, E. J. Cussen, D. Bradshaw, M. J. Rosseinsky, K. M. Thomas, *J. Am. Chem. Soc.* **2004**, *126*, 9750.
- [43] T. Fujimori, A. Morelos-Gómez, Z. Zhu, H. Muramatsu, R. Futamura, K. Urita, M. Terrones, T. Hayashi, M. Endo, S. Y. Hong, *Nat. Commun.* **2013**, *4*, 2162.
- [44] Y. Zhang, Z. Gao, N. Song, X. Li, *Electrochim. Acta* **2016**, *222*, 1257.
- [45] R. Brudler, H. J. M. de Groot, W. B. S. van Liemt, P. Gast, A. J. Hoff, J. Lugtenburg, K. Gerwert, *FEBS Lett.* **1995**, *370*, 88.
- [46] P. D. Lewis, K. E. Lewis, R. Ghosal, S. Bayliss, A. J. Lloyd, J. Wills, R. Godfrey, P. Kloer, L. A. Mur, *BMC Cancer* **2010**, *10*, 640.
- [47] G. Parthasarthy, M. Sevegney, R. M. Kannan, *J. Polym. Sci., Part B: Polym. Phys.* **2002**, *40*, 2539.
- [48] X. Colom, F. Carrillo, F. Nogués, P. Garriga, *Polym. Degrad. Stab.* **2003**, *80*, 543.
- [49] J. Tang, X. Jing, B. Wang, F. Wang, *Synth. Met.* **1988**, *24*, 231.
- [50] S.-N. Yuen, S.-M. Choi, D. L. Phillips, C.-Y. Ma, *Food Chem.* **2009**, *114*, 1091.
- [51] M. L. Duarte, M. C. Ferreira, M. R. Marvão, J. Rocha, *Int. J. Biol. Macromol.* **2002**, *31*, 1.
- [52] T. R. Devi, S. Gayathri, *Int. J. Pharm. Sci. Rev. Res.* **2010**, *2*, 106.
- [53] R. Seoudi, G. S. El-Bahy, Z. A. El Sayed, *J. Mol. Struct.* **2005**, *753*, 119.
- [54] S. J. Wen, T. J. Richardson, D. I. Ghantous, K. A. Striebel, P. N. Ross, E. J. Cairns, *J. Electroanal. Chem.* **1996**, *408*, 113.
- [55] N. M. Logacheva, V. E. Baulin, A. Y. Tsvadze, E. N. Pyatova, I. S. Ivanova, Y. A. Velikodny, V. V. Chernyshev, *Dalton Trans.* **2009**, 2482.
- [56] J. M. Thomas, I. Adams, R. H. Williams, M. Barber, *J. Chem. Soc., Faraday Trans. 2.* **1972**, *68*, 755.
- [57] G. Hollinger, P. Kumurdjian, J. M. Mackowski, P. Pertosa, L. Porte, T. M. Duc, *J. Electron. Spectrosc. Relat. Phenom.* **1974**, *5*, 237.
- [58] B. Lindberg, K. Hamrin, G. Johansson, U. Gelius, A. Fahlman, C. Nordling, K. Siegbahn, *Phys. Scr.* **1970**, *1*, 286.
- [59] a) B. J. Lindberg, K. Hamrin, G. Johansson, U. Gelius, A. Fahlman, C. Nordling, K. Siegbahn, *Phys. Scr.* **1970**, *1*, 286; b) J. A. Gardella Jr, S. A. Ferguson, R. L. Chin, *Appl. Spectrosc.* **1986**, *40*, 224.
- [60] Z. Zhao, S. Wang, R. Liang, Z. Li, Z. Shi, G. Chen, *J. Mater. Chem. A* **2014**, *2*, 13509.
- [61] M. Xiao, M. Huang, S. Zeng, D. Han, S. Wang, L. Sun, Y. Meng, *RSC Adv.* **2013**, *3*, 4914.
- [62] a) G. Ma, F. Huang, Z. Wen, Q. Wang, X. Hong, J. Jin, X. Wu, *J. Mater. Chem. A* **2016**, *4*, 16968; b) P. J. Hanumantha, B. Gattu, O. Velikokhatnyi, M. K. Datta, S. S. Damle, P. N. Kumta, *J. Electrochem. Soc.* **2014**, *161*, A1173; c) C. Liang, N. J. Dudney, J. Y. Howe, *Chem. Mater.* **2009**, *21*, 4724.
- [63] a) X. Liang, C. Hart, Q. Pang, A. Garsuch, T. Weiss, L. F. Nazar, *Nat. Commun.* **2015**, *6*, 5682; b) C. Zu, Y. Fu, A. Manthiram, *J. Mater. Chem. A* **2013**, *1*, 10362; c) Y.-S. Su, Y. Fu, T. Cochell, A. Manthiram, *Nat. Commun.* **2013**, *4*, 2985; d) C. Zu, N. Azimi, Z. Zhang, A. Manthiram, *J. Mater. Chem. A* **2015**, *3*, 14864; e) P. Murugavel Shanthi, P. Jampani Hanumantha, T. Albuquerque, B. Gattu, P. N. Kumta, *ACS Appl. Energy Mater.* **2018**, *1*, 483.
- [64] J. Jin, Z. Wen, G. Ma, Y. Lu, K. Rui, *Solid State Ionics* **2014**, *262*, 170.
- [65] S. Dapoz, N. Betz, M.-J. Guittet, A. Le Moël, *Nucl. Instrum. Methods Phys. Res., Sect. B* **1995**, *105*, 120.
- [66] J. Riga, P. Snauwaert, A. De Pryck, R. Lazzaroni, J. P. Boutique, J. J. Verbist, J. L. Brédas, J. M. André, C. Taliani, *Synth. Met.* **1987**, *21*, 223.
- [67] D. R. Huntley, *J. Phys. Chem.* **1992**, *96*, 4550.
- [68] F. Qin, K. Zhang, J. Fang, Y. Lai, Q. Li, Z. Zhang, J. Li, *New J. Chem.* **2014**, *38*, 4549.
- [69] Z. Li, L. Yuan, Z. Yi, Y. Liu, Y. Xin, Z. Zhang, Y. Huang, *Nanoscale* **2014**, *6*, 1653.
- [70] a) M. Barber, J. A. Connor, M. F. Guest, I. H. Hillier, M. Schwarz, M. Stacey, *J. Chem. Soc., Faraday Trans. 2.* **1973**, *69*, 551; b) D. Feng, Z. Zhou, M. Bo, *Polym. Degrad. Stab.* **1995**, *50*, 65; c) T. Nakayama, K. Inamura, Y. Inoue, S. Ikeda, K. Kishi, *Surf. Sci.* **1987**, *179*, 47.
- [71] S. Aduru, S. Contarini, J. W. Rabalais, *J. Phys. Chem.* **1986**, *90*, 1683.
- [72] H. U. Hummel, W. Förner, K. Krogmann, *Z. Anorg. Allg. Chem.* **1986**, *540*, 300.
- [73] S. Lalitha, P. Manoharan, *J. Electron Spectrosc. Relat. Phenom.* **1989**, *49*, 61.
- [74] E. Z. Kurmaev, V. V. Fedorenko, V. R. Galakhov, S. Bartkowski, S. Uhlenbrock, M. Neumann, P. R. Slater, C. Greaves, Y. Miyazaki, *J. Supercond.* **1996**, *9*, 97.
- [75] C. D. Wagner, J. A. Taylor, *J. Electron Spectrosc. Relat. Phenom.* **1982**, *28*, 211.
- [76] a) C. Bellitto, M. Bonamico, V. Fares, P. Imperatori, S. Patrizio, *J. Chem. Soc. Dalton Trans.* **1989**, *4*, 719; b) M. M. Chehimi, M. Delamar, *J. Electron Spectrosc. Relat. Phenom.* **1989**, *49*, 231.
- [77] a) W. Yao, Z. Zhang, J. Gao, J. Li, J. Xu, Z. Wang, Y. Yang, *Energy Environ. Sci.* **2009**, *2*, 1102; b) X. Li, Z. Yin, X. Li, C. Wang, *Ionic* **2014**, *20*, 795.
- [78] L.-F. Liao, C.-F. Lien, J.-L. Lin, *Phys. Chem. Chem. Phys.* **2001**, *3*, 3831.
- [79] L. Pereira, A. Sousa, H. Coelho, A. M. Amado, P. J. A. Ribeiro-Claro, *Biomol. Eng.* **2003**, *20*, 223.
- [80] S. Strawn, J. White, G. Marshall, L. Gee, H. Goodis, S. Marshall, *J. Dent.* **1996**, *24*, 417.
- [81] Z. Li, W.-T. Jiang, H. Hong, *Spectrochim. Acta, Part A* **2008**, *71*, 1525.
- [82] B. Mohammadi, A. A. Yousefi, S. M. Bellah, *Polym. Test.* **2007**, *26*, 42.
- [83] Y. Peng, P. Wu, *Polymer* **2004**, *45*, 5295.
- [84] H. Yang, G. V. Zhuang, P. N. Ross, *J. Power Sources* **2006**, *161*, 573.
- [85] M. Ludvigsson, J. Lindgren, J. Tegenfeldt, *Electrochim. Acta* **2000**, *45*, 2267.
- [86] P. Hassanzadeh, L. Andrews, *J. Am. Chem. Soc.* **1992**, *114*, 83.
- [87] C. Rao, R. Venkataraghavan, T. Kasturi, *Can. J. Chem.* **1964**, *42*, 36.
- [88] H. Yadav, N. Sinha, B. Kumar, *Mater. Res. Bull.* **2015**, *64*, 194.
- [89] Z. Slavkova, O. Kostadinova, G. Avdeev, T. Petkova, *Advanced Nanotechnologies for Detection and Defence against CBRN Agents*, Springer, Berlin/New York **2018**, pp. 87–93.